ADVANCED MATERIALS
www.advmat.de

Excitonic Aharonov–Bohm Oscillations in Core–Shell Nanowires

Pierre Corfdir, Oliver Marquardt, Ryan B. Lewis, Chiara Sinito, Manfred Ramsteiner, Achim Trampert, Uwe Jahn, Lutz Geelhaar, Oliver Brandt,* and Vladimir M. Fomin*

Phase coherence in nanostructures is at the heart of a wide range of quantum effects such as Josephson oscillations between exciton–polariton condensates in microcavities, conductance quantization in 1D ballistic transport, or the optical (excitonic) Aharonov–Bohm effect in semiconductor quantum rings. These effects only occur in structures of the highest perfection. The 2D semiconductor heterostructures required for the observation of Aharonov–Bohm oscillations have proved to be particularly demanding, since interface roughness or alloy fluctuations cause a loss of the spatial phase coherence of excitons, and ultimately induce exciton localization. Experimental work in this field has so far relied on either self-assembled ring structures with very limited control of shape and dimension or on lithographically defined nanorings that suffer from the detrimental effects of free surfaces. Here, it is demonstrated that nanowires are an ideal platform for studies of the Aharonov–Bohm effect of neutral and charged excitons, as they facilitate the controlled fabrication of nearly ideal quantum rings by combining all-binary radial heterostructures with axial crystal-phase quantum structures. Thanks to the atomically flat interfaces and the absence of alloy disorder, excitonic phase coherence is preserved even in rings with circumferences as large as 200 nm.

Nanowires are quasi-1D objects in which heterostructures can be fabricated both in the axial and radial direction.[1–4] Moreover, GaAs-based nanowires exhibit pronounced polytypism, i.e., they invariably form axial polytype heterostructures in which exciton confinement is achieved by an alternation of the crystal structure rather than by compositional changes.[5] Combining such axial crystal-phase quantum structures with compositional heterostructures in the radial direction results in the formation of quantum rings with highly reproducible electronic properties.[6]

Here, we report on the observation of the excitonic Aharonov–Bohm effect[7–11] in nanowire-based quantum rings that were designed by combining radial compositional and axial crystal-phase heterostructures. A schematic of the investigated nanowire structure is depicted in **Figure 1**a. The all-binary GaAs/AlAs radial quantum well structure is realized by synthesizing core–multishell nanowires. Under the specific growth conditions chosen in this work (see the Experimental Section), the nanowire core forms in the zincblende structure, but undergoes spontaneous rotational twinning during its axial growth.[12] The twin segments are separated by a twin boundary that acts as a 2 monolayer thick wurtzite segment in a zincblende matrix. As depicted in Figure 1b, this wurtzite segment forms a type II heterostructure that leads to an axial localization of excitons with an electron–hole overlap as large as 0.15.[5] Since the twin boundary extends into the shells during radial growth and thus intersects the GaAs shell quantum well, a quantum ring forms at the intersection (Figure 1a).[6]

The Aharonov–Bohm effect results from the phase shift acquired by an electronic excitation in a ring threaded by a magnetic field, and is in essence a property of charged particles.[12–14] However, the effect also occurs for excitons in quantum rings if they exhibit a radial polarization,[8–10,14,15] so that the flux of an external magnetic field through the orbits defined by the electron and hole wavefunctions (Ψ_e and Ψ_h, respectively) is different. Increasing the magnetic field gives rise to oscillations in the exciton energy and oscillator strength characterized by a period B_C[16]

$$B_C = \frac{\Phi_0}{\pi \left| \langle r_e^2 \rangle - \langle r_h^2 \rangle \right|} \tag{1}$$

Dr. P. Corfdir,[+] Dr. O. Marquardt, Prof. R. B. Lewis, Dr. C. Sinito,[++]
Dr. M. Ramsteiner, Dr. A. Trampert, Dr. U. Jahn, Dr. L. Geelhaar, Dr. O. Brandt
Paul-Drude-Institut für Festkörperelektronik
Leibniz-Institut im Forschungsverbund Berlin e. V.
Hausvogteiplatz 5–7, 10117 Berlin, Germany
E-mail: pierre.corfdir@pdi-berlin.de; oliver.brandt@pdi-berlin.de
Dr. O. Marquardt
Weierstraß-Institut für Angewandte Analysis und Stochastik
Leibniz-Institut im Forschungsverbund Berlin e. V.
Mohrenstraße 39, 10117 Berlin, Germany
Prof. V. M. Fomin
Institute for Integrative Nanosciences
Leibniz IFW Dresden
Helmholtzstraße 20, 01069 Dresden, Germany
The ORCID identification number(s) for the author(s) of this article can be found under https://doi.org/10.1002/adma.201805645.
[+]Present address: ABB Corporate Research, 5405 Baden-Dättwil, Switzerland
[++]Present address: Attolight AG, EPFL Innovation Park, Bât. D, 1015 Lausanne, Switzerland

DOI: 10.1002/adma.201805645

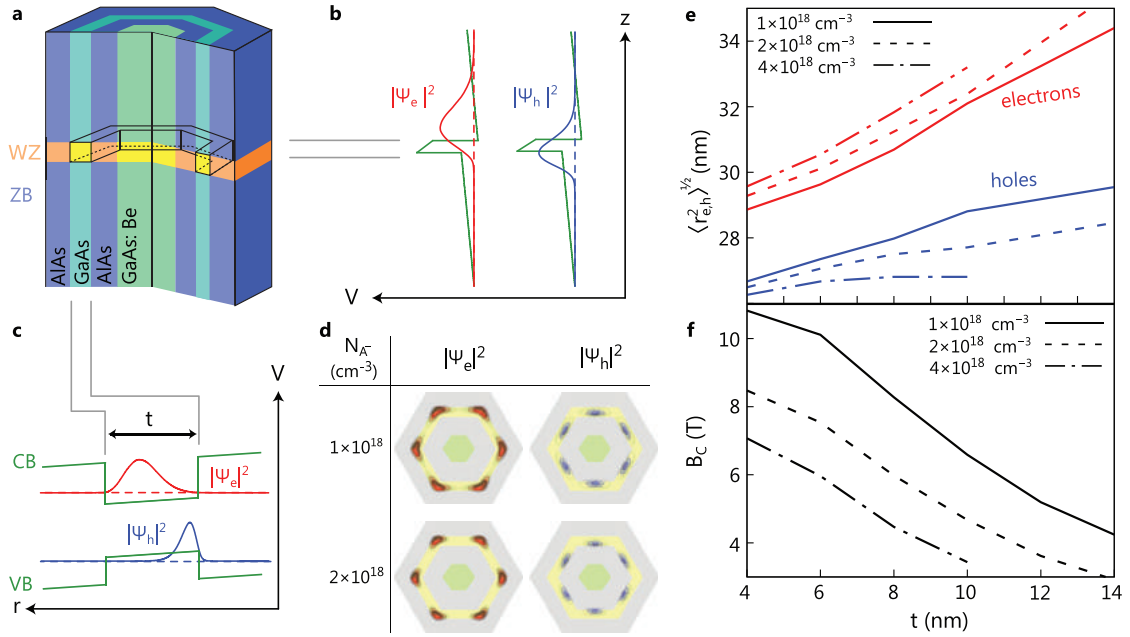

Figure 1. Electronic properties of quantum rings in GaAs/AlAs core–multishell nanowires. a) Schematic representation of the GaAs/AlAs core–multishell nanowire under investigation. The zincblende (ZB) GaAs core (green) exhibits a diameter of 30 nm and is doped with Be. The GaAs shell quantum well (turquoise) with a width t is clad by AlAs shells (blue) with a thickness of 15 nm, sufficiently thick to prevent the tunneling of charge carriers from the quantum well shell to the core. A wurtzite (WZ) segment created by a twin boundary propagates through the entire diameter of the nanowire (orange and yellow). The quantum ring formed by the intersection of the shell quantum well and the twin boundary is highlighted. b,c) Schematic representation of the conduction and valence band edges in the axial (b) and radial (c) directions with the associated electron (red) and hole (blue) ground state charge densities. d) Distribution of electron (red) and hole (blue) charge density across the section of the quantum ring for a nanowire with $t = 7$ nm and two different ionized acceptor concentrations N_{A^-} in the core. e) Root mean square radii of the electron (red) and hole (blue) charge densities as a function of t for three different ionized acceptor concentrations as indicated in the figure. f) Characteristic magnetic field B_C that induces a 2π phase shift to the exciton wave function, as a function of t for the same ionized acceptor concentrations as in (e).

with the magnetic flux quantum $\Phi_0 = 2\pi\hbar/e$ and the expectation values $\langle r_e^2 \rangle^{1/2}$ and $\langle r_h^2 \rangle^{1/2}$ of the electron and hole radii calculated with Ψ_e and Ψ_h, respectively. Figure 1c shows the band profile of the GaAs shell quantum well with a Be-doped GaAs core, which induces an electric field in the quantum well. The resulting radial separation of Ψ_e and Ψ_h is determined by the quantum well width t and the ionized acceptor concentration N_{A^-}.

The optical observation of Aharonov–Bohm oscillations requires on the one hand a delocalized exciton in the quantum ring with a sufficiently large electron–hole overlap to facilitate the detection of optical transitions associated with the recombination of the exciton. On the other hand, B_C has to be experimentally accessible, and should thus not exceed a few T. Consequently, a compromise between the intensity of the excitonic transitions and their B_C has to be found. We have identified appropriate values for both t and N_A by 3D simulations using an eight band $\mathbf{k}\cdot\mathbf{p}$ model (see the Experimental Section) for the nanowire depicted in Figure 1a. Figure 1d displays $|\Psi_{e,h}|^2$ for $t = 7$ nm and $N_{A^-} = 1$ and 2×10^{18} cm^{-3}. In both cases, the electrons (holes) are located at the edge (center) of the facets. The exciton wavefunction, which is essentially given by $\Psi_e\Psi_h$, is thus delocalized around the quantum ring, while $\langle r_e^2 \rangle^{1/2}$, $\langle r_h^2 \rangle^{1/2}$, and B_C depend sensitively on t as well as on N_{A^-} as shown in Figures 1e,f, respectively. For $t > 10$ nm and $N_{A^-} = 4 \times 10^{18}$ cm^{-3}, B_C is predicted to approach values lower than 4 T (Figure 1f). However, the increasing radial separation of electrons and holes for thicker wells (Figure 1c) and the rising electron concentration at the vertices of the hexagonal quantum ring for higher doping levels (Figure 1d) reduce the electron–hole overlap, which may eventually inhibit the radiative decay of the exciton. Furthermore, the well width has to be chosen such that the emission of the quantum ring is spectrally distinct from that of the core.

Guided by these results and considerations, GaAs/AlAs core–multishell nanowires were fabricated by Ga-assisted vapor–liquid solid growth in molecular beam epitaxy (see the Experimental Section). Be was used as the acceptor with a nominal concentration in the low 10^{18} cm^{-3} range. The cores were subject to a partial thermal decomposition after growth to reduce the core diameter to values of 20–30 nm.[17,18] **Figure 2** shows scanning electron microscopy images of: a) Be-doped GaAs cores after partial thermal decomposition and b) the complete GaAs/AlAs core–multishell nanowires used for detecting Aharonov–Bohm oscillations, respectively. The nanowires are separated by over 1 µm, allowing us to access single nanowires optically. Figure 2c displays transmission-mode scanning electron microscopy images of single nanowires from (left) the as-grown Be-doped cores and (right) the complete core–multishell structure. The axial contrast variations originate from the presence of rotational twin segments in the nanowires, and are seen to persist in the core–shell nanowires.[11] The plan-view transmission electron microscopy images in Figure 2d confirm that the core and shell dimensions of the nanowires are close

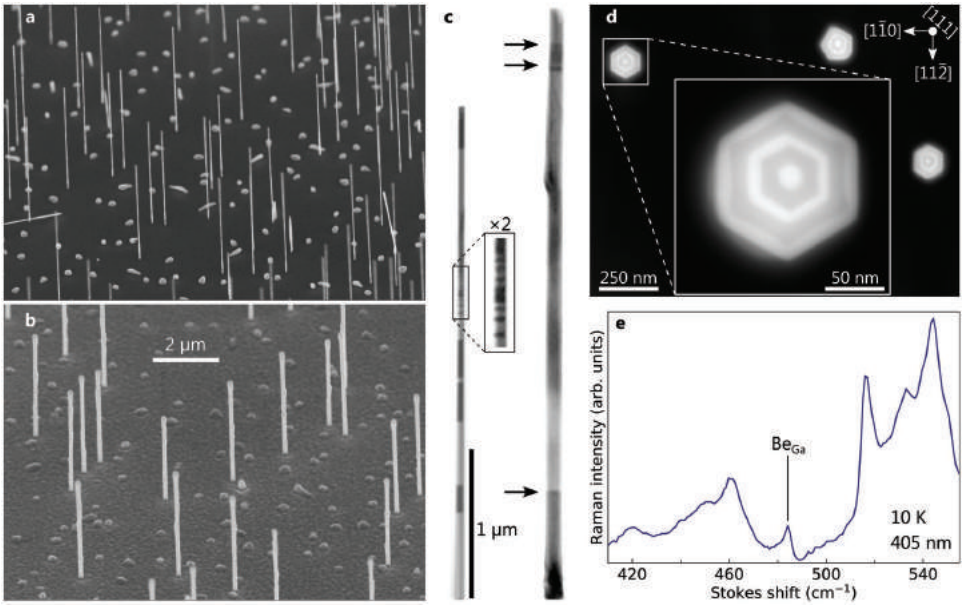

Figure 2. Morphology, microstructure, and doping of GaAs/AlAs core–multishell nanowires. a,b) Bird's eye view scanning electron microscopy images of two different nanowire ensembles. a) An ensemble of ultrathin Be-doped GaAs cores obtained by partial thermal decomposition of GaAs nanowires grown by molecular beam epitaxy on Si(111). b) The full GaAs/AlAs core–multishell nanowires used for the spectroscopic investigation of the Aharonov–Bohm effect. The scale bar applies to both microscopy images. c) Transmission-mode scanning electron microscopy images of (left) a GaAs core prior to the partial thermal decomposition process and (right) a full GaAs/AlAs core–multishell nanowire after partial thermal decomposition of the GaAs core and radial regrowth of the GaAs and AlAs shells. The contrast variations along the nanowires axis indicate the presence of twin segments. The inset shows a magnified view of multiple nanotwins with a minimum length below 10 nm. The arrows point out selected twin boundaries. d) Plan-view high-angle annular dark-field transmission electron microscopy image of a few GaAs/AlAs core–multishell nanowires from the ensemble depicted in (b). GaAs and AlAs appear bright and dark, respectively. For the nanowire shown in the magnified view in the inset, the core diameter [(20 ± 2) nm] as well as the thicknesses of the AlAs and GaAs shells [(15 ± 2) and (8 ± 2) nm, respectively] are close to the nominal values (see the Experimental Section). e) Raman spectrum of an ultrathin Be-doped GaAs nanowire at 10 K. The spectrum is dominated by various bands due to intrinsic second-order phonon scattering in GaAs. The line at 484 cm^{-1} stems from a local vibrational mode associated with Be on Ga sites (Be_{Ga}).

to the designated values. Finally, Figure 2e displays a Raman spectrum detected on a single Be-doped core. The intensity of the local vibrational mode for Be_{Ga} indicates a Be concentration between 3 and 6×10^{18} cm^{-3}.[19]

Figure 3a shows low-temperature photoluminescence spectra of the nanowire ensemble depicted in Figure 2b. Independent of excitation density, the spectra are dominated by a band centered at 1.503 eV that arises from the recombination of excitons bound to twin boundaries in the GaAs core of the nanowires.[5,20] A band centered at 1.623 eV is detected on the high-energy side of the core emission. The energy of this band has been found to decrease with increasing quantum well thickness (not shown), revealing that it originates from the recombination of excitons confined in the GaAs shell quantum well. Since the twin boundaries formed in the core also extend into the shells (Figure 2c), this high-energy band is likely to be dominated by recombination of quantum well excitons bound to twin boundaries, or, in other words, excitons in quantum ring states.[6] Figures 3b,c show photoluminescence spectra taken on two different single nanowires (NW1 and NW2, respectively) at 4.2 K. The transition energies indicate shell quantum wells with a width of $t = 7$ nm. The full width at half maximum of these lines is typically between 200 and 500 μeV, smaller than reported for GaAs crystal-phase quantum wells,[21] larger than those of crystal-phase quantum dots,[22,23] and comparable to those reported for GaAs-based quantum wires obtained by post-growth lithography techniques.[8,24] Hence, we attribute the narrow transitions in the spectra to single quantum rings.

A magneto-photoluminescence map taken on NW1 for magnetic fields between 0 and 8 T is shown in Figure 3d. Selected spectra extracted from this image are displayed in Figure 3e. With increasing magnetic field, the transition seen in Figure 3b splits and shifts, as a result of Zeeman and diamagnetic effects. The evolution of the transition energies with increasing magnetic field is, however, not parabolic, but rather exhibits an oscillatory behavior with the split states oscillating in phase. This observation is in striking contrast to the monotonic dependence observed for a reference sample with undoped core (Figure S1, Supporting Information). Figure 3f shows the evolution of the average energy of the Zeeman split states with magnetic field as determined by line-shape fits shown in Figure 3e. The oscillations of the average energy in Figure 3f are consistent with the optical Aharanov–Bohm effect. To extract B_C for this quantum ring, we fit the magnetic field-dependence of the energy in Figure 3f with a parabola modulated by a sine function. The best fit yields a diamagnetic coefficient $\gamma = -2.9$ μeV T^{-2} and $B_C = 2.2$ T. For NW2, we obtain $B_C = 3.1$ T and $\gamma = 1.5$ μeV T^{-2} in an analogous fashion (Figure 3g). The values found for B_C are similar to those reported in refs. [8,9] for GaAs-based quantum rings with diameters of about 40 nm. Note that despite the simplicity

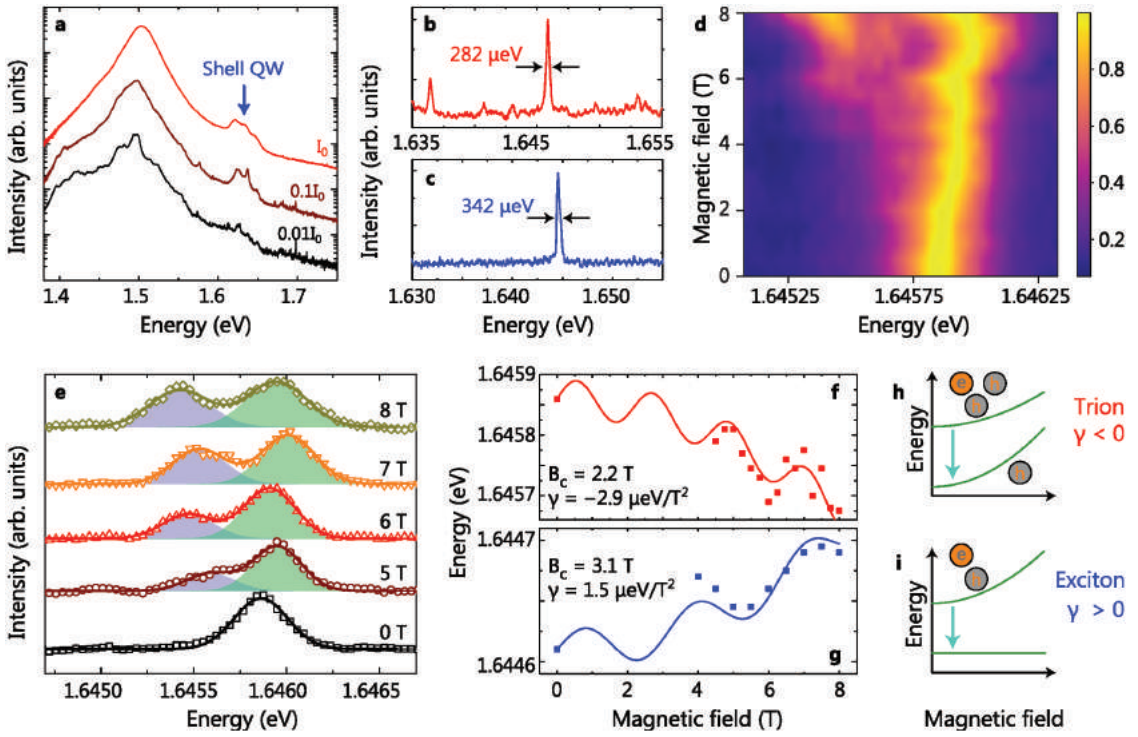

Figure 3. Optical Aharanov–Bohm oscillations in GaAs/AlAs crystal-phase quantum rings. a) Photoluminescence spectra taken on an ensemble of GaAs/AlAs core–multishell nanowires at 10 K. The relative excitation power is specified for each spectrum. The bands at 1.503 and 1.623 eV arise from the exciton recombination at twin boundaries in the GaAs core and shell quantum well, respectively. b,c) Photoluminescence spectra recorded from nanowire NW1 (b) and nanowire NW2 (c). The full width at half maximum of the photoluminescence lines is below 500 μeV, suggesting that they originate from excitons in single quantum rings. d) Evolution of the exciton energy in a magnetic field for the quantum ring in NW1. The magnetic field is parallel to the nanowire axis. The spectra have been normalized and their intensity is color-coded according to the scale bar. e) Photoluminescence spectra at selected magnetic fields (symbols) from NW1. The spectra have been normalized and shifted vertically for clarity. The lines are the results of Gaussian fits. The blue and green shaded areas highlight the contribution of each Zeeman split state to the spectrum. f,g) Dependence of the average energy of the Zeeman split states on magnetic field for the rings in NW1 (f) and NW2 (g). Data points are shown only for *B* fields large enough for the two split states to be resolved. The solid lines are fits accounting for Aharonov–Bohm oscillations and a diamagnetic shift. h,i) Schematic representation of the energy of the initial and final states involved in the radiative decay of a charged (h) and a neutral (i) exciton as a function of the magnetic field. The transition energy for the charged and neutral excitons decreases and increases with increasing magnetic field, respectively.

of our model, the B_C values measured for NW1 and NW2 are within a factor of two from those predicted in Figure 1f for structures with $N_{A^-} = 4 \times 10^{18}$ cm^{-3} and $t = 7$ nm. The opposite sign of γ for NW1 and NW2 indicates that the nature of the excitonic complexes responsible for the respective transitions is different. As shown in Figures 3h,i, the energy of both charged and neutral excitons increases with increasing magnetic field. The energy of both electrons and holes, being the final state for the recombination of charged excitons, exhibits an even stronger increase (Figure 3h).[25] The transition energy of a trion thus decreases in the presence of a magnetic field, and γ is negative, as observed in Figure 3f. In contrast, the transition energy of the neutral exciton increases, giving rise to a positive γ, as seen in Figure 3g. We suggest that the trion in NW1 is a positively charged exciton, with an extra hole originating from an ionized acceptor in the GaAs core of the nanowires.

These results demonstrate that GaAs/AlAs core–shell nanowires do not only possess the structural perfection required for the observation of phase-coherence effects, but also offer a high degree of control over dimensions and doping level. These nanowires thus open a unique way toward wavefunction engineering in 3D quantum structures for the experimental study of excitonic phase coherence phenomena.

Experimental Section and Simulations

Simulations: Electron and hole ground state wave functions and energies were obtained using a 3D eight-band $\mathbf{k}\cdot\mathbf{p}$ model within the plane-wave based multiphysics library S/Phi/nX.[26,27] The GaAs/AlAs core–multishell configuration depicted in Figure 1a was considered, assuming a Be-doped GaAs core of 30 nm diameter and AlAs shells of 15 nm thickness cladding a GaAs shell quantum well whose width was varied between 4 and 14 nm (the outermost GaAs shell that served to protect the AlAs shell from oxidation was not included in the calculations since it has negligible impact on the electronic properties of the structure). The core was assumed to be fully depleted and to exhibit ionized acceptor concentrations N_{A^-} of 1×10^{18}, 2×10^{18} cm^{-3}, or 4×10^{18} cm^{-3}. The resulting radial band bending was obtained by separately solving the Poisson equation in cylindrical coordinates for a homogeneous charge distribution. Twin boundaries in the zincblende can be considered as wurtzite segments with a thickness of 2 monolayers. To reduce the number of elements in the simulation mesh and to reduce the computational effort, the twin boundary was

represented by a 4 monolayer thick wurtzite segment, leading only to an insignificant change of the energy of the associated confined state. The axial wurtzite segment was placed in the center of a 10 nm long zincblende segment of the core–shell structure. Strain due to the lattice mismatch between GaAs and AlAs as well as between the zincblende and wurtzite modifications was taken into account. Furthermore, the resulting piezoelectric polarization was considered together with the spontaneous polarization in the wurtzite segment.

Sample Fabrication: Samples were grown by molecular beam epitaxy on p-type Si(111) wafers covered by native oxide. The growth system was equipped with effusion cells for Ga, Al, and Be, as well as a valved cracker for producing As_2. First, Ga droplets were formed on the substrate by depositing Ga for 30 s at 0.37 nm s^{-1} GaAs equivalent growth rate, followed by a 60 s anneal.[28] Subsequently, GaAs nanowire cores of length, diameter and density of about 4 µm, 60 nm and 0.3 μm^{-2}, respectively, were grown by supplying Ga and As_2 at 0.085 and 0.71 nm s^{-1} equivalent GaAs growth rates, respectively, along with Be. The substrate temperature during core synthesis was 645 °C, as measured by a pyrometer calibrated to the oxide desorption temperature of GaAs(001). Resistivity measurements on nanowires grown with the same Be and Ga fluxes—corresponding to a hole density of 10^{19} cm^{-3} for planar growth on GaAs(100)—were consistent with a nanowire doping level of about 10^{18} cm^{-3}. Following core growth, the Ga droplets on top of the nanowires were converted to GaAs by exposure to As_2 at 1.1 nm s^{-1}, and the nanowires were subsequently decomposed for 5 min at 680 °C in the absence of any flux, which reduced the nanowire diameter from 60 to 20–30 nm.[17] Finally, GaAs and AlAs shells were deposited at 480 °C with nominal thicknesses of 7.5 and 15 nm, respectively. To prevent the oxidation of the outer AlAs shell, the nanowires were finally covered by a 10 nm thick GaAs shell. The substrate was rotated with 10 revolutions per minute throughout the entire growth process. For comparison, a sample was grown with the same structure, but without Be core doping (Figure S1, Supporting Information).

Electron Microscopy: Bird's eye view secondary electron microscopy images of the as-grown nanowire ensembles were recorded with a Hitachi S-4800 field emission microscope using an acceleration voltage of 5 kV and a magnification of 10000 ×. Transmission-mode scanning electron microscopy images from single nanowires were obtained in a Zeiss Ultra-55 field emission microscope using an acceleration voltage of 20 kV and a magnification of 30000 ×. For transmission electron microscopy, cross-sections of the nanowires perpendicular to the growth axis were prepared by first embedding the free-standing wires in glue for mechanical stabilization followed by conventional polishing and Argon ion beam sputtering down to electron transparency. Scanning transmission electron microscopy was performed by using a JEOL 2100F field emission instrument equipped with a bright-field and a dark-field detector and operated at 200 kV. The core–shell nanowire structures were oriented along the ⟨111⟩ crystallographic direction parallel to the electron beam. High angle annular dark-field images were recorded with an inner and outer collection angle of 70 and 180 mrad to be sensitive to the chemical composition of AlAs and GaAs, respectively.

Optical Spectroscopy: Photoluminescence (PL) experiments on an ensemble of nanowires at 10 K were carried out with the 632.8 nm line of a HeNe laser as excitation source. The samples were mounted on the coldfinger of a continuous-flow He cryostat, and the laser beam was focused using a microscope objective with a numerical aperture of 0.25. The PL was dispersed with an 80 cm focal length monochromator equipped with a 600 lines mm^{-1} grating and detected with a liquid N_2-cooled charge-coupled device (CCD). In this experiment, the excitation power I_0 corresponded to 0.6 mW. For measurements at 4.2 K, the samples were kept at liquid He temperature in an attoLiquid 1000 bath cryostat equipped with a confocal optical setup. A 650 nm laser diode was used as excitation source, and the laser beam was focused using a microscope objective with a numerical aperture of 0.82. The PL signal was collected using the same objective and coupled to a multimode fiber with a core diameter of 25 µm. The signal was dispersed with a 55 cm focal length monochromator equipped with a 1800 lines mm^{-1} grating and detected with a liquid N_2-cooled CCD. Magnetic fields B with a strength between 0 and 8 T could be applied in Faraday configuration, i.e., $B \| \langle 111 \rangle$. Raman scattering measurements were performed at low temperature (10 K) in backscattering geometry with the light wavevector perpendicular to the side facets of nanowires dispersed on a gold-coated Si substrate. For optical excitation, the 405 nm line of a laser diode was focused by a microscope objective onto the nanowires. The backscattered light was collected by the same objective, spectrally dispersed by an 80 cm focal length monochromator equipped with a 2400 lines mm^{-1} grating and detected with a liquid-N_2-cooled CCD.

Supporting Information

Supporting Information is available from the Wiley Online Library or from the author.

Acknowledgements

The authors would like to thank Doreen Steffen for preparing the samples for transmission electron microscopy, Anne-Kathrin Bluhm for additional scanning electron microscopy, Jesús Herranz for nanowire resistivity measurements, Michael Höricke and Carsten Stemmler for maintenance of the molecular beam epitaxy system, Jonas Lähnemann for help with the data analysis, and Stefan Fölsch and Gabriel Christmann for a critical reading of the manuscript. P. C. is grateful to the Fonds National Suisse de la Recherche Scientifique for funding through project 161032. O. M. is indebted to the Deutsche Forschungsgemeinschaft for support within the collaborative research center 787 Semiconductor Nanophotonics under grant B4. R.B.L. acknowledges funding from the Alexander von Humboldt foundation. Figure 1d was prepared using VMD.[29]

Conflict of Interest

The authors declare no conflict of interest.

Keywords

3D nanostructures, core–shell nanowires, excitonic Aharonov–Bohm effect, phase coherence

Received: August 30, 2018
Revised: October 15, 2018
Published online:

[1] M. S. Gudiksen, L. J. Lauhon, J. Wang, D. C. Smith, C. M. Lieber, *Nature* **2002**, *415*, 617.
[2] M. Björk, B. Ohlsson, T. Sass, A. Persson, C. Thelander, M. Magnusson, K. Deppert, L. Wallenberg, L. Samuelson, *Appl. Phys. Lett.* **2002**, *80*, 1058.
[3] Y. Wu, R. Fan, P. Yang, *Nano Lett.* **2002**, *2*, 83.
[4] L. J. Lauhon, M. S. Gudiksen, D. Wang, C. M. Lieber, *Nature* **2002**, *420*, 57.
[5] P. Corfdir, B. Van Hattem, E. Uccelli, S. Conesa-Boj, P. Lefebvre, A. Fontcuberta i Morral, R. T. Phillips, *Nano Lett.* **2013**, *13*, 5303.
[6] P. Corfdir, R. B. Lewis, O. Marquardt, H. Küpers, J. Grandal, E. Dimakis, A. Trampert, L. Geelhaar, O. Brandt, R. T. Phillips, *Appl. Phys. Lett.* **2016**, *109*, 082107.
[7] A. V. Chaplik, *JETP Lett.* **1995**, *62*, 900.
[8] E. Ribeiro, A. O. Govorov, W. Carvalho, G. Medeiros-Ribeiro, *Phys. Rev. Lett.* **2004**, *92*, 126402.

[9] A. E. Hansen, A. Kristensen, S. Pedersen, C. B. Sørensen, P. E. Lindelof, *Phys. Rev. B* **2001**, *64*, 045327.
[10] M. Bayer, M. Korkusinski, P. Hawrylak, T. Gutbrod, M. Michel, A. Forchel, *Phys. Rev. Lett.* **2003**, *90*, 186801.
[11] F. Ding, N. Akopian, B. Li, U. Perinetti, A. Govorov, F. M. Peeters, C. C. Bof Bufon, C. Deneke, Y. H. Chen, A. Rastelli, O. G. Schmidt, V. Zwiller, *Phys. Rev. B* **2010**, *82*, 075309.
[12] *Physics of Quantum Rings* (Ed.: V. M. Fomin), Springer Science & Business Media, Berlin/Heidelberg, Germany **2014**.
[13] W.-H. Lin, U. Jahn, H. Küpers, E. Luna, R. B. Lewis, L. Geelhaar, O. Brandt, *Nanotechnology* **2017**, *28*, 415703.
[14] G. Timp, A. M. Chang, J. E. Cunningham, T. Y. Chang, P. Mankiewich, R. Behringer, R. E. Howard, *Phys. Rev. Lett.* **1987**, *58*, 2814.
[15] A. Fuhrer, S. Lüscher, T. Ihn, T. Heinzel, K. Ensslin, W. Wegscheider, M. Bichler, *Nature* **2001**, *413*, 822.
[16] This result is obtained in an idealized case, where electron and hole wavefunctions are approximated by infinitely narrow 1D rings with radii equal to the root mean square radii for the actual 3D wave functions.
[17] B. Loitsch, D. Rudolph, S. Morkötter, M. Döblinger, G. Grimaldi, L. Hanschke, S. Matich, E. Parzinger, U. Wurstbauer, G. Abstreiter, J. J. Finley, G. Koblmüller, *Adv. Mater.* **2015**, *27*, 2195.
[18] J. K. Zettler, P. Corfdir, C. Hauswald, E. Luna, U. Jahn, T. Flissikowski, E. Schmidt, C. Ronning, A. Trampert, L. Geelhaar, H. T. Grahn, O. Brandt, S. Fernández-Garrido, *Nano Lett.* **2016**, *16*, 973.
[19] M. Hilse, M. Ramsteiner, S. Breuer, L. Geelhaar, H. Riechert, *Appl. Phys. Lett.* **2010**, *96*, 193104.
[20] M. Heiss, S. Conesa-Boj, J. Ren, H.-H. Tseng, A. Gali, A. Rudolph, E. Uccelli, F. Peiró, J. R. Morante, D. Schuh, E. Reiger, E. Kaxiras, J. Arbiol, A. Fontcuberta i Morral, *Phys. Rev. B* **2011**, *83*, 045303.
[21] A. M. Graham, P. Corfdir, M. Heiss, S. Conesa-Boj, E. Uccelli, A. Fontcuberta i Morral, R. T. Phillips, *Phys. Rev. B* **2013**, *87*, 125304.
[22] N. Akopian, G. Patriarche, L. Liu, J.-C. Harmand, V. Zwiller, *Nano Lett.* **2010**, *10*, 1198.
[23] M. Bouwes Bavinck, K. D. Jöns, M. Zieliński, G. Patriarche, J.-C. Harmand, N. Akopian, V. Zwiller, *Nano Lett.* **2016**, *16*, 1081.
[24] H. Kim, W. Lee, S. Park, K. Kyhm, K. Je, R. A. Taylor, G. Nogues, L. S. Dang, J. D. Song, *Sci. Rep.* **2017**, *7*, 40026.
[25] A. V. Chaplik, V. M. Kovalev, *New Versions of the Aharonov-Bohm Effect in Quantum Rings* (Ed.: V. M. Fomin), Springer Science & Business Media, Berlin/Heidelberg, Germany **2014**, pp. 199–245.
[26] O. Marquardt, S. Boeck, C. Freysoldt, T. Hickel, S. Schulz, J. Neugebauer, E. P. O'Reilly, *Comput. Mater. Sci.* **2014**, *95*, 280.
[27] S/Phi/nX website, https://sxrepo.mpie.de (accessed: October 2018).
[28] H. Küpers, F. Bastiman, E. Luna, C. Somaschini, L. Geelhaar, *J. Cryst. Growth* **2017**, *459*, 43.
[29] W. Humphrey, A. Dalke, K. Schulten, *J. Mol. Graph.* **1996**, *14*, 33.